Earth and Planetary Science Letters 273 (2008) 115–122

Contents lists available at ScienceDirect

Earth and Planetary Science Letters

journal homepage: www.elsevier.com/locate/epsl

α–β–γ transformations in Mg_2SiO_4 in Earth's transition zone

Yonggang G. Yu [a,*], Zhongqing Wu [b], Renata M. Wentzcovitch [b]

[a] Department of Chemistry, Minnesota Supercomputing Institute, University of Minnesota, Minneapolis, MN 55455, USA
[b] Department of Chemical Engineering and Materials Science, Minnesota Supercomputing Institute, University of Minnesota, Minneapolis, MN 55455, USA

ARTICLE INFO

Article history:
Received 31 October 2007
Received in revised form 3 June 2008
Accepted 11 June 2008
Available online 26 June 2008

Editor: R.D. van der Hilst

Keywords:
phase transition
forsterite
wadsleyite
ringwoodite
transition zone

ABSTRACT

Phase relations in α–β–γ Mg_2SiO_4 have been investigated by first principles quasi-harmonic free energy computations. The computed phase boundaries obtained using the local density approximation (LDA) and the generalized gradient approximation (GGA) bracket the experimental ones, with LDA (GGA) calculations giving the lowest (highest) bound, while the Clapeyron slopes are in good agreement with the experimentally determined ones. This is the same trend displayed by previous similar computations. Further analyses reveal that despite the uncertainties in phase boundary determination, the calculated discontinuities in density, bulk modulus, and bulk sound velocity are quite insensitive to pressure and have small uncertainties and useful accuracy to discriminate potential sources of discontinuities in the mantle. We verify that ~3% density discontinuity at 410-km depth can be produced primarily by the α to β transition in an aggregate with pyrolite composition, i.e. ~60 vol.% of Mg_2SiO_4. However, the 1.3–2.9% density discontinuity observed in some places at 520-km depth cannot be accounted for solely by the β to γ transition but also requires changes in the coexisting pyroxene/garnet/Ca-perovskite system.

1. Introduction

Olivine, α-, wadsleyite, β-, and ringwoodite, γ-$(Mg,Fe)_2SiO_4$, are the most abundant minerals of the upper mantle and transition zone. A phase transformation between the α and β polymorphs (Ringwood and Major, 1970) is generally believed to cause the major discontinuity in density and velocities at 410-km depth defining the boundary between the upper mantle and the transition zone in Earth. This boundary is relatively sharp, i.e., ~5 km wide, and there is much consensus about its origin and the magnitude of the discontinuities there (for a review see Agee, 1998). Laboratory measurements of acoustic wave velocities in individual phases (Li and Liebermann, 2007) and simultaneous calculations of thermodynamic equilibrium in mantle aggregates (Ita and Stixrude, 1992) support the view that an upper mantle with approximately pyrolite composition, i.e. ~60 vol.% olivine can produce the 410-km discontinuity. It has been known for a long time (Ringwood, 1975) that the β to γ transition in Mg_2SiO_4 could contribute to the high velocity gradient in the mid-transition zone region; another expected contribution to this high gradient is produced by the (Mg, Fe, Ca)gt→(Mg, Fe)gt+Ca-perovskite reaction. Since then there has been a rich and extensive literature in mineral physics trying to elucidate phase equilibria conditions and phase transformations in the olivine system (e.g., Suito, 1977; Yagi et al., 1979; Akaogi et al., 1984; Price et al., 1987; Akaogi et al., 1989; Katsura and Ito, 1989; Chopelas, 1991; Stixrude and Bukowinski, 1993; Morishima et al., 1994; Suzuki et al., 2000; Inoue et al., 2006) and in the garnet-form system (e.g., Irifune et al., 1989; Canil, 1994; Koito et al., 2000; Weidner and Wang, 2000) to better understand seismic observations in the mid-transition zone. There are also controversial seismic observations of fine structure features around 520-km depth. Using long or short period data some seismic studies found global (e.g., Wiggins and Helmberger, 1973; Shearer, 1990; Revenaugh and Jordan, 1991) or regional (e.g., Ryberg et al., 1997) evidence for the 520-km discontinuity, but others did not find convincing evidence (e.g., Jones et al., 1992) for this discontinuity. Some other studies using underside reflection data in the mantle did not find the 520-km discontinuity universally detectable (Gossler and Kind, 1996; Gu et al., 1998). Some seismic study also reported the 520-km discontinuity splits into two discontinuities at 500- and 560-km (Deuss and Woodhouse, 2001).

Previous modelling studies of the $(Mg,Fe)_2SiO_4$ phase diagram (Akaogi et al., 1984; Price et al., 1987; Akaogi et al., 1989; Chopelas, 1991; Stixrude and Bukowinski, 1993; Stixrude and Lithgow-Bertelloni, 2005a) reproduced well the experimentally observed phase boundaries. These studies were enlightening but depended in one way or another upon limited experimental data such as high-temperature calorimetric data (Akaogi et al., 1989), limited vibrational properties obtained from infrared and Raman measurements (Akaogi et al., 1984; Chopelas, 1991), or parameterized thermodynamic models (Stixrude and Bukowinski, 1993; Stixrude and Lithgow-Bertelloni, 2005a), or upon parameterized interatomic potentials (Price et al., 1987). Nowadays density functional based (Kohn and Sham, 1965) quasi-harmonic computations are commonly used to predict high P–T thermodynamic properties with considerable accuracy (Karki et al., 2000a,b; Yu and Wentzcovitch, 2006; Li et al., 2007; Wu and Wentzcovitch, 2007). Phase boundaries can also be predicted but with relatively larger uncertainties in pressure (Tsuchiya et al., 2004; Yu

* Corresponding author. Tel.: +1 612 624 2872; fax: +1 612 626 7246.
E-mail address: yonggang@cems.umn.edu (Y.G. Yu).

0012-821X/$ – see front matter © 2008 Elsevier B.V. All rights reserved.
doi:10.1016/j.epsl.2008.06.023

et al., 2007), however they can still provide useful insights. In this paper, we investigate by first principles the α–β–γ sequence of transformations in iron-free Mg_2SiO_4 and present subtle details of property changes across these transformations. We then address the mineralogical origin of the 410-km and 520-km discontinuities in light of these results.

2. Computational details

Complete thermodynamic calculations in iron-free olivine, wadsleyite, and ringwoodite have been performed using the plane-wave pseudopotential method in conjunction with the quasi-harmonic approximation (QHA) (Yu and Wentzcovitch, 2006; Li et al., 2007; Wu and Wentzcovitch, 2007). Details about the pseudopotentials' parameters and experimental data on these minerals are given in those papers and references therein. Very encouraging agreement with experimental measurements in thermodynamic properties at relevant mantle P–Ts has been reported for each phase. Differences between calculations and experiments were shown to be less than 2% for Raman and IR frequencies, 0.3% for volume, 2% for thermal expansivity, 0.5% for adiabatic bulk moduli, and 4% for temperature derivative of bulk moduli at upper mantle conditions. Those previous LDA studies on α-, β-, and γ-Mg_2SiO_4 have chosen difference k-point sampling in static self-consistent calculations, i.e., 2×2×2 (1 point), 2×2×2 (4 points), and 4×4×4 (10 points), with (1/2 1/2 1/2) shift from the origin. To ensure accurate static transition pressure, commensurate and fully converged k-point sampling and a sufficiently large kinetic energy cutoff (E_{cut}) must be used to calculate the static energy of fully relaxed crystal structures. Therefore, we refined those static calculations using an E_{cut} of 70 Ry and denser k-point meshes of 4×2×4 (16 points), 4×4×4 (17 points), and 4×4×4 (10 points) with (1/2 1/2 1/2) shift from the Γ-point (Monkhorst and Pack, 1976) for α, β, and γ phases, respectively. The final energy convergence with respect to E_{cut} and k-point mesh was estimated to be within 2.5×10^{-4} Ry per formula unit. All structures were well optimized (Wentzcovitch, 1991) until the net forces on all ions were less than 5×10^{-5} Ry/Bohr and the stress less than 10^{-4} Ry/Bohr^3. Full phonon dispersion in the first Brillouin zone including the vibrational density of states (VDoS) was calculated by the density functional perturbation theory (Baroni et al., 2001).

Within the QHA, the Helmholtz free energy is expressed as

$$F(V,T) = U_0(V) + \frac{1}{2}\sum_{\mathbf{q},j}\hbar\omega_j(\mathbf{q},V) + k_BT\sum_{\mathbf{q},j}\ln\left[1-\exp\left(-\hbar\omega_j(\mathbf{q},V)/k_BT\right)\right], \quad (1)$$

in which U_0 (V) is the static DFT internal energy at volume V and $\omega_j(\mathbf{q},V)$ represents the jth phonon frequency with wave number $\mathbf{q}$ in the Brillouin zone. The second and third terms in Eq. (1) represent lattice vibrational zero point motion and thermal excitation energies respectively. Once VDoS was calculated at several volumes we obtained the Helmholtz free energy (F) at these volumes (V) in a fine temperature (T) grid. Then a fourth order finite strain equation of state was fitted at each T yielding F on a V–T grid. Using the finite difference method all thermodynamic properties, including the Gibbs free energy (G), were derived numerically from F on this V–T grid and later on were inverted into a pressure–temperature (P–T) grid with spacings of 0.1 GPa and 10 K. Besides, any point inside this grid could be interpolated whenever needed. Finally the phase boundary was found by comparing $G(P,T)$ of two different phases.

Our calculation shows that static energy convergence with respect to k-point sampling was insufficient in a previous study of forsterite by Li et al. (2007). We find that changing k-point mesh from (2×2×2) to (4×2×4), both with (1/2 1/2 1/2) shift from origin, increases the LDA static energy by ~10 meV/atom. The insufficient k-point sampling of previous study increased the α–β static transition pressure (P_{tr}^{static}) by 3 GP, such that the LDA calculated P_{tr}^{static} for the α–β transition becomes larger than P_{tr}^{static} for the β–γ transition, which is erroneous. We calculated the free energy in the α phase until the phase boundary converged. Fortunately only a negligible difference with respect to Li et al.'s (2007) results is found for VDoS and derivatives of the free energy at high P–T. Comparison of thermodynamic properties obtained in this study (LDA), in Li et al. (2007) (LDA), and in experimental measurements is shown in Table B.1. At high P–T, this calculation in forsterite agrees very well with experimental measurements in volume, thermal expansion coefficient, bulk modulus, and heat capacity. Energy convergences with respect to k-point sampling in previous studies of β and γ phases (Yu and Wentzcovitch, 2006; Wu and Wentzcovitch, 2007) was confirmed. Since previous studies of α-, β-, and γ-Mg_2SiO_4 reported only the LDA results, we obtained also the GGA counterpart for each phase in this study. This allowed for a comparative study of phase transitions by the LDA and GGA functionals.

3. α–β–γ phase boundaries

Shown in Fig. 1 are the calculated differences of static enthalpy versus pressure by the local density approximation (LDA, Ceperley and Alder, 1980) and the generalized gradient approximation (GGA, Perdew et al., 1996) functionals. The GGA transition pressures are ~6 GPa higher than the LDA ones. Specifically, $P_{\alpha-\beta}^{LDA}$=6.5 GPa, $P_{\alpha-\beta}^{GGA}$=12.6 GPa, $P_{\beta-\gamma}^{LDA}$=9.6 GPa, and $P_{\beta-\gamma}^{GGA}$=15.7 GPa. This is a consequence of differences in the LDA and GGA functional forms (Asada and Terakura, 1992; Yu et al., 2007). The uncertainties in total energies cause uncertainties of ~0.1 GPa in these transition pressures. A comparison of calculated results with calorimetric measurements (Akaogi et al., 1984, 1989) of molar volume, enthalpy, and entropy changes across the α–β and β–γ transitions is shown in Table 1. Overall GGA results compare more favorably with the data for the α–β transition. For the β–γ transition GGA and LDA results compare equally well with the data. The relatively large experimental uncertainties and the non-systematic trends in these comparisons make it difficult to pin down the reason why the LDA and GGA phase boundaries bracket the experimental ones (see below).

Both α–β and β–γ phase boundaries have positive Clapeyron slopes (CS). The Clapeyron equation $\frac{dP}{dT} = \frac{\Delta S}{\Delta V}$ states that if entropy decreases across a phase transition, i.e. $\Delta S<0$, then the phase boundary has a positive CS since $\Delta V<0$ for a pressure-induced transition. The decrease in entropy from α to β to γ can be understood from changes in VDoS of the three phases. Within the QHA, entropy is given by

$$S(V,T) = k_B\sum_{q,i}\left[\frac{\hbar\omega_{q,i}(V)/k_BT}{\left(e^{\frac{\hbar\omega_{q,i}(V)}{k_BT}}-1\right)} - \ln\left(1-e^{-\frac{\hbar\omega_{q,i}(V)}{k_BT}}\right)\right]. \quad (2)$$

S decreases with the overall increase in phonon frequencies or with an increase in the center of mass, ω_{cm}, of the VDoS (Navrotsky, 1980).

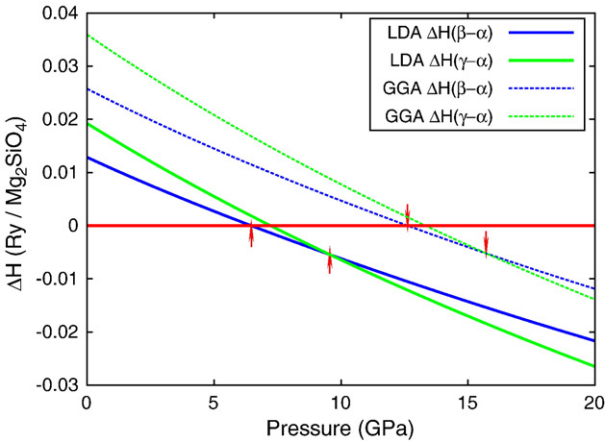

Fig. 1. Static enthalpy differences between forsterite (α), wadsleyite (β), and ringwoodite (γ) Mg_2SiO_4 versus pressure calculated by the LDA and GGA.

Table 1
Comparison of calculated and experimentally measured enthalpy, entropy, and molar volume changes for α–β–γ transitions in Mg_2SiO_4 (1 formula unit)

Transition		ΔV_{298} (cm^3/mol)	ΔH_{975} (J/mol)	ΔS_{975} (J/(mol·K))
α–β	exp[a]	−3.16	–	−7.7±1.9
	exp[b]	−3.13	29,970±2840	−10.5±2.1
	LDA	−2.95	17,452	−8.6
	GGA	−3.34	32,767	−9.5
β–γ	exp[a]	−0.98	9080±2120	−7.3±1.4
	exp[b]	−0.89	6820±3766	−6.3±3.8
	LDA	−1.04	7078	−4.1
	GGA	−1.13	13,204	−4.9
α–γ	exp[a]	−4.14	39,050±2620	−15.0±2.4
	exp[b]	−4.02	36,777±3724	−16.7±2.9
	LDA	−4.00	24,530	−12.7
	GGA	−4.47	45,971	−14.4

[a] exp data from Table 3 in Akaogi et al. (1989).
[b] exp data from Table 2 in Akaogi et al. (1984).

The VDoS for the three phases at 15 GPa, shown in Fig. 2, indicates a sequential increase in the low-frequency edge of the VDoS and a decrease in the high-frequency edge. The lowest frequencies consist primarily of MgO bond stretching modes and the highest frequencies are primarily SiO bond stretching modes. At 15 GPa the MgO and SiO bond-lengths decrease and increase, respectively, along the α–β–γ phase sequence. The black dots indicate the positions of ω_{cm} of the these distributions (Fig. 2). They are respectively 513, 518, and 523 cm^{-1} for the α, β, and γ phases. The decrease in entropy throughout this phase sequence is related to this increase in ω_{cm}.

We proceed to derive the LDA and GGA phase boundaries. They are displayed in solid lines in Fig. 3(a) for the α–β and in 3(b) for the β–γ transition. For both transitions, experimentally determined phase boundaries are bracketed by the LDA and GGA results. The GGA boundaries are somewhat closer to the experimental boundaries than the LDA ones, in both cases. Similar results were observed in other calculations using the same pseudopotentials (Tsuchiya et al., 2004; Yu et al., 2007). Our calculated LDA (GGA) CSs are 2.7 (2.5) MPa/K and 3.6 (3.5) MPa/K for the α–β and β–γ transitions, respectively. Despite the uncertainties in the phase boundaries related to the exchange correlation functionals, we find CSs in quite good agreement with measured values — 1.8–4.0 MPa/K (α–β transition) and 4.1–6.9 MPa/K (β–γ transition) (Akaogi et al., 1989; Katsura and Ito, 1989; Morishima et al., 1994; Suzuki et al., 2000; Katsura et al., 2004; Inoue et al., 2006), and with previous quasi-harmonic calculations — 2.7 MPa/K (α–β transition) (Price et al., 1987; Chopelas, 1991). See Fig. 3 caption for more detailed citations.

Recent phase equilibria study on a homogeneous upper mantle aggregate (Stixrude and Lithgow-Bertelloni, 2005a) produced a CS consistent with that found by Morishima et al. (1994) (3.6±0.2 MPa/K). The difference between our calculation and theirs may reflect the intrinsic difference between the QHA free energy using the DFT calculated phonon DoS and the free energy derived from the effective Debye model and the Grüneisen approximation (Stixrude and Lithgow-Bertelloni, 2005b). Nevertheless, our CS might have been underestimated by use of the QHA. For instance, in forsterite anharmonic effects are well known (e.g., Gillet et al., 1991). This effect, not included in the QHA, could increase the CS and/or shift the phase boundary at high temperatures. Fig. 3 indicates that the regime of validity of the QHA, determined on the basis of the criterion requiring the second derivative of the thermal expansivity to vanish (Wentzcovitch et al., 2004), does not encompass the entire temperature range of experiments and anharmonicities could be the cause of the discrepancy between our results and experiments. However, the expected *P*–*T* conditions (the mantle geotherm Brown and Shankland, 1981) at the 410- and 520-km discontinuities fall marginally within the QHA regime of validity. The broadening of the QHA validity

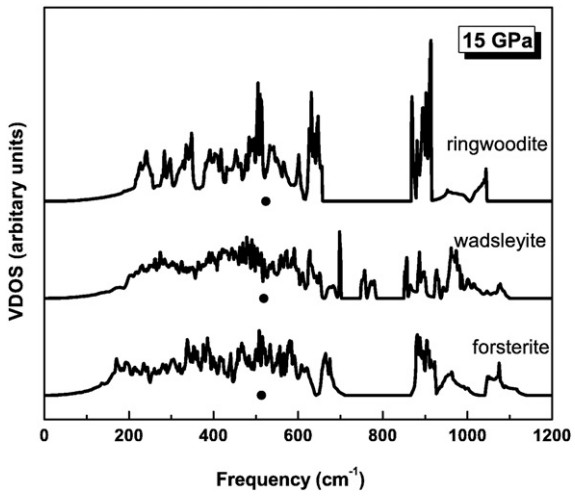

Fig. 2. Vibrational density of states of forsterite (α), wadsleyite (β), and ringwoodite (γ) Mg_2SiO_4 at 15 GPa. The black dots denote ω_{cm}s, the average (center of mass) frequencies, which are 513, 518, and 523 cm^{-1} for α, β, and γ, respectively.

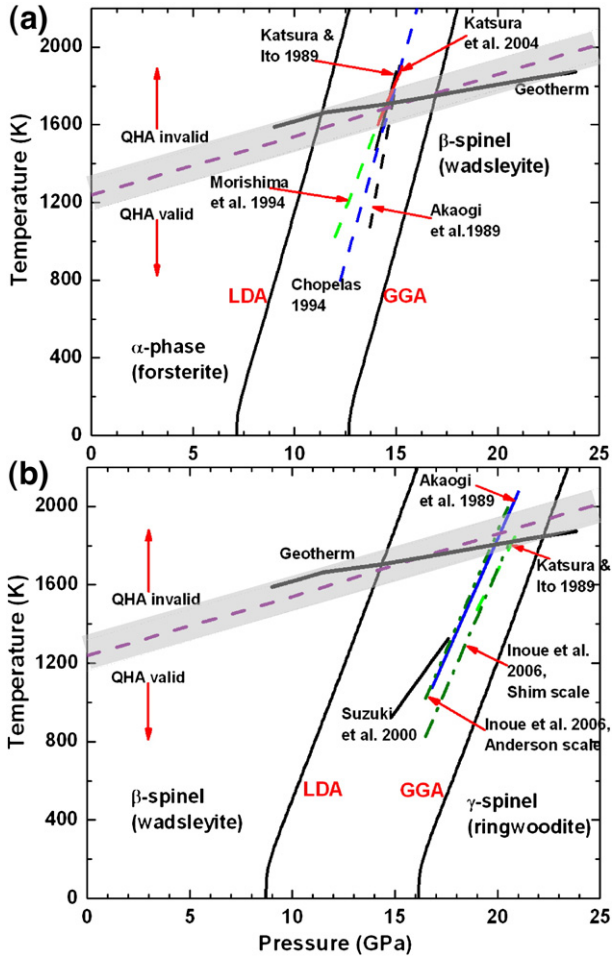

Fig. 3. Calculated phase boundaries compared with experiments. (a) For the α–β transition, the Clapeyron slopes (at ~1500 K) in MPa/K are: 2.5 (GGA), 2.7 (LDA), 2.5 (Katsura and Ito, 1989), 1.8 (Akaogi et al., 1989), 2.7 (Chopelas, 1991), 3.6 (Morishima et al., 1994), 4.0 (Katsura et al., 2004). (b) For the β–γ transition, the Clapeyron slopes (at ~1700 K) are in MPa/K: 3.5 (GGA), 3.6 (LDA), 4.4 (Katsura and Ito, 1989), 4.2 (Akaogi et al., 1989), 4.1 (Inoue et al., 2006), 6.9 (Suzuki et al., 2000). The mantle geotherm is based on the estimate by Brown and Shankland (1981). The QHA validity limit is estimated from the inflection point on the thermal expansivity curve (see Section 3).

limit in Fig. 3 is caused by a numerical uncertainty related with the determination of $|(\partial^2\alpha/\partial T^2)_P| < \varepsilon$, where $\varepsilon \approx 10^{-12}$ K^{-3}.

We summarize in Fig. 4 the phase stability field of α, β, γ Mg_2SiO_4 and MgO (periclase) + $MgSiO_3$ (perovskite) found by LDA and GGA. LDA gives a qualitatively correct sequence of phase transitions under pressure, but transition pressures are about 5–15 GPa smaller than the experimental values. In contrast, GGA phase boundaries seem to agree much better with experiments (data from Katsura and Ito, 1989; Ito and Takahashi, 1989), but still offer transition pressures ~3 GPa higher. This trend, valid at least for silicate minerals, should be kept in mind for future reference. Fig. 4 also shows the dissociation of wadsleyite into MgO + pv at high temperatures (>2000 K). The calculated β–γ–(MgO + pv) coexisting point occurs at 2020 K and 22.8 GPa, which is close to that found by Stixrude and Bukowinski (1993, Fig. 4), i.e., 2000 K and 21.5 GPa. The CSs found for β and γ dissociation are ~ −1.7 and −2.9 MPa/K (GGA), respectively. The former differs from the CS found by Stixrude and Bukowinski (1993) (~ −3.0 MPa/K). This difference may originate in the distinct phonon density of states used by these calculations. The calculated CS for the γ dissociation transition is consistent with experimental values by Ito and Takahashi (1989), Akaogi and Ito (1993), Irifune et al. (1998), Shim et al. (2001), and Chudinovskikh and Boehler (2001), i.e., −2.9 to −2.6 MPa/K, but differs from the more recent results, e.g. Katsura et al. (2003), Fei et al. (2004), Litasov et al. (2005), reporting smaller values, i.e., −1.3 to −0.4 MPa/K. We hope to document more phase boundaries with this type of calculation in the future to establish by systematic comparison with experiments the degree of reliability of this method.

Regarding the accuracy related to these phase boundary calculations, within the framework of LDA or GGA the estimated uncertainty in static transition pressure is ~0.6 GPa and uncertainty in the CS is ~0.3 MPa/K. The errors caused by pseudopotentials and by the finite difference method as used here should be small, which in some sense is demonstrated by the good agreement between experiments and calculations of the α-, β-, and γ-Mg_2SiO_4 phases' properties. The error stemming from the use of the QHA has not been estimated. But we have been very stringent in determining the range of validity of the QHA. The error associated with the QHA should not invalidate our conclusions regarding density discontinuities (see next section), which is very robust, even though it might change the location of the phase boundaries and the CSs.

Previous studies of the thermodynamic properties of each one of these phases of Mg_2SiO_4 (Yu and Wentzcovitch, 2006; Li et al., 2007; Wu and Wentzcovitch, 2007), MgO (Karki et al., 2000b), and $MgSiO_3$ (Karki et al., 2000a) have established that the LDA predicts much better structural properties, e.g., volume, bulk modulus, etc., than the GGA, even though the latter appears to offer somewhat better values for ΔH, ΔG, and P_{tr} than the former (Fig. 1 and Table 1). Hence we will use the LDA to compute property changes across the GGA phase boundaries, unless otherwise specified.

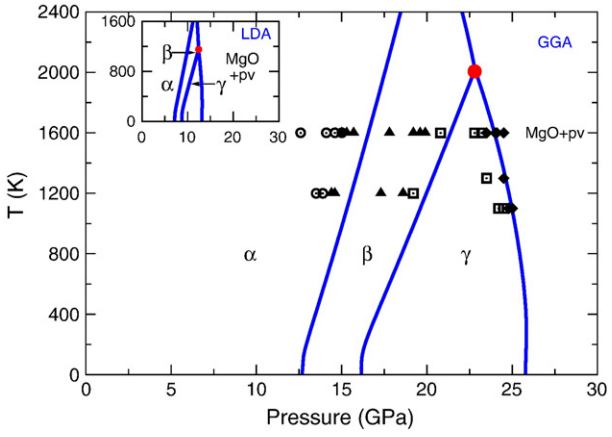

Fig. 4. Phase stability fields of α-, β-, γ-Mg_2SiO_4, and MgO + $MgSiO_3$-pv. ⊙: α phase, ▲: β phase, ⊡: γ phase, ◆: MgO + pv. Experimental data from Katsura and Ito (1989), Ito and Takahashi (1989).

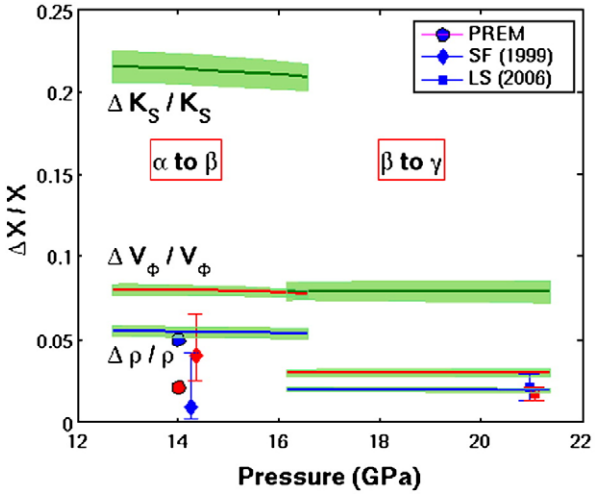

Fig. 5. Calculated changes, $\Delta x/x$ in ρ, K_S, and V_Φ (defined in Section 4) along the GGA boundaries in Fig. 3. The lower (upper) bound in the green shaded areas represents property change calculated by the LDA (GGA) functional. Temperature varies with pressure as indicated along the phase boundaries. PREM = Dziewonski and Anderson (1981), SF = Shearer and Flanagan (1999), and LS = Lawrence and Shearer (2006). (For interpretation of the references to color in this figure legend, the reader is referred to the web version of this article.)

4. Discontinuities across α–β–γ phase transitions in Mg_2SiO_4 and in mantle aggregates

We define a property discontinuity across a phase transition as $\Delta x/x \equiv (x_B - x_A)/[(x_B + x_A)/2]$, with x being ρ, K_S, or V_Φ $\left(V_\Phi = \sqrt{K_S/\rho}\right)$. Here A denotes the low-pressure phase α (β), and B denotes the high-pressure phase β (γ). The calculated $\Delta x/x$ using the LDA (GGA) functional along the GGA phase boundaries (Fig. 3) provides the lower (upper) bound of the green shaded areas in Fig. 5, while the middle solid line represents an average of the two bounds. For the α–β transition we find $\Delta\rho/\rho = 5.1\%$, $\Delta V_\Phi/V_\Phi = 7.6\%$, and $\Delta K_S/K_S = 22\%$ at ~1500 K. For the β–γ transition we find $\Delta\rho/\rho = 1.8\%$, $\Delta V_\Phi/V_\Phi = 2.7\%$, and $\Delta K_S/K_S = 7.2\%$ at ~1700 K (Table 2 and Fig. 5). Properties discontinuities produced by the β–γ transition are considerably smaller than those produced by the α–β transition. One notable feature shown in Table 2 is that $\rho^{\beta\text{-}Mg_2SiO_4} < \rho_{PREM}$ and $K_S^{\beta\text{-}Mg_2SiO_4} > K_S^{PREM}$ at P–T conditions between 410- and 520-km depth. This difference is expected to be compensated when pyroxene/garnet/(Ca–perovskite) system is added to the aggregate which has not been included at this stage.

As is well known in the transition zone, pyroxenes, garnets, and Ca-perovskite (Ca-pv) coexist with the Mg_2SiO_4 polymorphs. These phases also undergo phase transitions (Ringwood, 1975) but they seem to occur within much wider pressure ranges (e.g., Gasparik, 1990) compared to the transitions we are addressing, even in the presence of the binary loops caused by the (Mg,Fe) solid solutions in the α, β, and γ phases (Katsura and Ito, 1989). These wide transitions alter substantially density and velocity gradients in Earth's transition zone, but whether or not they cause any sharp discontinuity is still not completely clear (Ita and Stixrude, 1992). Here we calculate the density discontinuities produced in mantle aggregates with variable olivine volume fractions under the assumption that sharp phase transitions occur only in the olivine system. We compare these density discontinuities with the seismically observed values at 410-km and 520-km depth despite the fact that seismic data at 520-km depth are more controversial than those at 410-km depth. We then check the consistency of the pyrolite compositional model and of the presumed cause of these mantle discontinuities.

Table 2
The LDA calculated Mg_2SiO_4 properties along the GGA phase boundary for α–β transition (~1500 K, 16.3 GPa), and β–γ transition (~1700 K, 20.2 GPa), compared with 410- and 520-km seismic data and mineral physics experiments

		Calc. Mg_2SiO_4	PREM	Seismic data and mineral physics calc.
ρ (g/cm^3)	Upper 410-km (α)	3.47	3.54†	
	Lower 410-km (β)	3.65	3.72†	
	%Δ 410-km ($\alpha\rightarrow\beta$)	5.1%	5.0%†	0.2–4.2% (a, seismic)
	Upper 520-km (β)	3.70	3.85§	
	Lower 520-km (γ)	3.77	–	
	%Δ 520-km ($\beta\rightarrow\gamma$)	1.8%	–	1.3–2.9% (b, seismic) 2.5–3.0% (c, Mg_2SiO_4) 2.5% (d, $(Mg_{0.88}Fe_{0.12})_2SiO_4$)
K_S (GPa)	Upper 410-km (α)	178.3	173.5†	
	Lower 410-km (β)	218.3	189.9†	
	%Δ 410-km ($\alpha\rightarrow\beta$)	20.2%	9.0%†	
	Upper 520-km (β)	231.9	218.1§	
	Lower 520-km (γ)	249.5	–	
	%Δ 520-km ($\beta\rightarrow\gamma$)	7.3%	–	
V_Φ (km/s)	Upper 410-km (α)	7.17	7.00†	
	Lower 410-km (β)	7.73	7.14†	
	%Δ 410-km ($\alpha\rightarrow\beta$)	7.6%	1.9%†	1.5–6.6% (a, seismic)
	Upper 520-km (β)	7.91	7.54§	
	Lower 520-km (γ)	8.13	–	
	%Δ 520-km ($\beta\rightarrow\gamma$)	2.7%	–	1.3–2.1% (b, seismic)

Here $\%\Delta=\Delta x/x_{av}$, $\Delta x=x_B-x_A$, and $x_{av}=(x_B+x_A)/2$, with $x=\rho$, K_S, and V_Φ. A denotes α (β) and B denotes β (γ) for the 410-km (520-km) transition. † = Preliminary Reference Earth Model (PREM, Dziewonski and Anderson, 1981) at 400-km and § = PREM at 500-km, (a)=Shearer and Flanagan (1999), (b)=Lawrence and Shearer (2006), (c)=Rigden et al. (1991), and (d)=Sinogeikin et al. (2003).

Under the above assumptions, the relative density change at 410-km (520-km) can be expressed as (see Appendix A)

$$\frac{\Delta\rho}{\rho}\equiv\frac{\rho_{B+others}-\rho_{A+others}}{(\rho_{B+others}+\rho_{A+others})/2}=\frac{2y}{\frac{2}{1-\theta}-y}. \quad (3)$$

Here A denotes the low-pressure phase α (β), and B denotes the high-pressure phase β (γ) at 410-km (520-km). $y=V_A/V_{A+others}$ is the phase A volume fraction in the aggregate; "others" means all mineral phases other than phase A or its transformed product, phase B. $\theta=V_B/V_A$ depends on the P–T conditions along the phase boundary. For instance, for the α–β transition, θ= 0.9504, 0.9506, and 0.9509 (0.9444, 0.9446, and 0.9448) at 1300, 1500, and 1700 K along the GGA (LDA) boundary; for the β–γ transition, θ=0.9822, 0.9823, and 0.9824 (0.9796, 0.9797, and 0.9798) at 1500, 1700, and 1900 K along the GGA (LDA) boundary. Therefore in general, $\Delta\rho/\rho$ is a function of y and T, with P being a dependent variable along the phase boundary. Eq. (3) indicates that iron and other alloy elements present in the aggregate will not alter the density discontinuity, if their presence does not change θ, the volume ratio between phases.

4.1. 410-km density discontinuity

The density discontinuity produced by the α–β transition at three different temperatures along the phase boundaries is shown in Fig. 6. The discontinuity is plotted against Mg_2SiO_4 volume fraction, y. The lower (upper) bounds of the shaded area in Fig. 6 correspond to density discontinuities calculated at 1300, 1500, and 1700 K along the GGA (LDA) boundary, while the middle dashed line represents $\Delta\rho/\rho$ calculated at 1500 K on the experimental boundary (Katsura and Ito, 1989). Based on this calculation, the 5% density increase, given by PREM, cannot be produced exclusively by the α–β transition, but requires simultaneous changes in the coexisting phases (unless the volume fraction of Mg_2SiO_4 is ~90%). However, the 0.2–4% density increase estimated by a seismic impedance study (Shearer and Flanagan, 1999) is fully consistent with the discontinuity predicted by Eq. (3) in a pyrolite-type model. For instance ~60 vol.% Mg_2SiO_4 in the transition zone would produce ~3.0% density increase (GGA boundary), which is in good agreement with the 2.9% estimate (Gaherty et al., 1999) for a pyrolite compositional model.

Nevertheless, because of the large uncertainties in $\Delta\rho/\rho$ derived from the seismic impedance study, this good agreement between predicted and observed density jump may be marginal. In the upper mantle pyroxene coexists with olivine and dissolves extensively into garnet over a large pressure range (~7–15 GPa at ~1200 °C). A drastic change in the proportion of pyroxene to garnet occurs near the end of the transformation (Ringwood, 1975; Akaogi and Akimoto, 1979; Irifune, 1987). This can produce a high velocity gradient between 300 and 460-km depth as pointed out by Ringwood (1975). But how influential Al and other elements, such as Ca and Fe, are in determining phase equilibrium in the pyroxene/garnet/Ca-pv system (solid-solid solution), e.g. determining the sharpness of the transition (Stixrude, 1997), is still unclear (e.g. Weidner and Wang, 2000). Furthermore whether or not this pyroxene-garnet transformation coincides with the α–β transition in Earth to produce 410-km discontinuity is an unresolved issue. Our understanding of the 410-km discontinuity will not be complete until the effects of Al and other elements such as Ca and Fe on the phase equilibrium are understood. We expect first principles based phase equilibrium calculations in the future will be able to shed light on this problem.

4.2. 520-km density discontinuity

During the past 20 yr or so, much knowledge has been accumulated about phase transitions and thermodynamic properties of transition zone minerals (see references in Stixrude and Lithgow-Bertelloni, 2005b; Li and Liebermann, 2007) and their aggregates (Ita and Stixrude, 1992; Stixrude and Lithgow-Bertelloni, 2005a). Density and velocity gradients calculated for an aggregate with pyrolite-type composition showed good agreement with seismic data (Ita and Stixrude, 1992; Li and Liebermann, 2007). It has been speculated that possible causes of the 520-km discontinuity comprise the β–γ transition in Mg_2SiO_4, clinopyroxene+majorite garnet to majorite garnet+Ca-pv transformation, and compositional change or layer (Agee, 1998). Lack of precise high P–T thermodynamic data in these key transition zone minerals, as well as accurate knowledge of the Ca content near 520-km depth and its partitioning in majorite garnet, rendered these hypotheses unclear, albeit much effort has been devoted to this issue (e.g., Duffy and Anderson, 1989; Gasparik, 1990; Revenaugh and Jordan, 1991). Next we show evidence that the β–γ

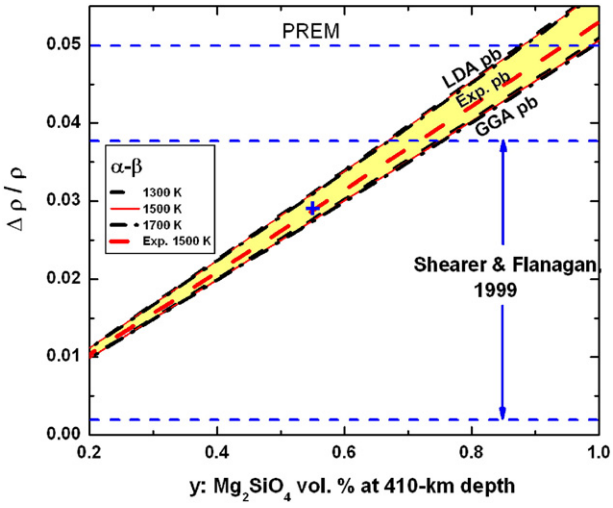

Fig. 6. Density discontinuity produced by the α–β transition in an aggregate with variable volume fraction of Mg_2SiO_4 (Section 4.1). Results are plotted for three points along the GGA, LDA, and experimental boundary by Katsura and Ito (1989) (Fig. 3(a)) and compared with PREM and with the seismic impedance study by Shearer and Flanagan (1999). The plus sign (+) indicates the pyrolite model based estimate of 410-km density discontinuity (Gaherty et al., 1999).

transition in Mg_2SiO_4 is unable to produce the 520-km discontinuity alone, thus emphasizing the importance of phase transitions in the pyroxene/garnet/Ca-pv system.

Fig. 7 shows the density discontinuity produced by the β–γ transition as a function of Mg_2SiO_4 volume fraction at 1500, 1700, and 1900 K along the GGA and LDA boundaries (Fig. 3(b)). $\Delta\rho/\rho$ at 1700 K on the experimental boundary (Katsura and Ito, 1989) is also calculated and shown by a dashed line in the middle of the shaded area in Fig. 7. One should note that $\Delta\rho/\rho$ calculated on the LDA boundary should be less accurate, because the LDA substantially underestimates P_{tr} by ~4 GPa (Fig. 3(b)). An aggregate with pyrolite composition, e.g., ~60 vol.% of Mg_2SiO_4, would produce only 1% density discontinuity (GGA boundary). The 1.3–2.9% density jump at 520-km depth inferred from an impedance study by Lawrence and Shearer (2006) cannot be explained by the β–γ transition alone in a pyrolite aggregate. This discontinuity would require at least 70 vol.% of Mg_2SiO_4 in the aggregate according to the calculated $\Delta\rho/\rho$ along the GGA or the experimental boundary (Fig. 7). This strongly suggests that the 520-km discontinuity needs to have contributions from phase transitions in the pyroxene/garnet/Ca-pv system.

The presence of iron and hydrogen in the aggregate is expected to have only a minor effect on the density discontinuity, although their effects on phase boundaries are more prominent (e.g., Ito and Takahashi, 1989; Matsuzaka et al., 2000; Ohtani and Litasov, 2006). If inverse spinel (O'Neill and Navrotsky, 1983) does coexist with normal spinel (γ phase), then the relative density discontinuity caused by the β–γ transition will decrease even further, because of the larger inverse spinel unit cell (Kiefer et al., 1999).

There is clear evidence that Ca-pv exsolves from garnet at ~1500 °C and 17–18 GPa (Gasparik, 1989; Canil, 1994), which can contribute to the density and velocity discontinuities at 520-km depth (Weidner and Wang, 2000). Our results verify arguments that it is indispensable to include the important impact of pyroxene/garnet/Ca-pv system upon the 520-km discontinuity, which presumably will change the width of this discontinuity also.

Recently a mineral physics interpretation (Saikia et al., 2008) of the 520-km discontinuity splitting (into 500- and 560-km) (Deuss and Woodhouse, 2001) has been proposed. It was suggested that the 500-km discontinuity should be assigned to the β–γ transition and the deeper discontinuity to the Ca-pv exsolution from garnet. Based on a phase equilibrium study combining mineral physics data, the authors also estimated the density discontinuity caused by the β–γ transition in fertile peridotite to be ~1.7%. This is in line with the study by Sinogeikin et al. (2003), who reported the density increase in $(Mg_{0.88}Fe_{0.12})_2SiO_4$ caused by β–γ transition to be 2.5%. Our calculated density discontinuity caused by the β–γ transition in pure Mg_2SiO_4 is 1.8% and our estimated density increase in a typical mantle aggregate (with 60 vol.% Mg_2SiO_4) is only ~1%. One should note that the experimental density at high P–T (e.g. Sinogeikin et al., 2003) used by Saikia et al. (2008) was extrapolated using a third-order Birch–Murnaghan equation of state (Birch, 1952). This extrapolation depends on both $(\partial M/\partial T)_P$, which was experimentally determined, and $\partial^2 M/\partial T\partial P$, which was not but was approximated using $g^M \equiv \partial \ln\left(\frac{\partial M}{\partial P}\right)_T/\partial\rho = -\frac{\partial^2 M}{\partial T\partial P}/\left(\left(\frac{\partial M}{\partial P}\right)_T \cdot \alpha\right) \approx -1$, with M being bulk or shear moduli (K_S or G). Our numerical calculation shows that g^{K_S} is material dependent, e.g., at 0 GPa $g^{K_S} \approx -0.7$, −1.2, and −0.5 for α-, β-, and γ-Mg_2SiO_4, respectively. Therefore it is not at all surprising that experimental extrapolations differ from our DFT results. We feel that the DFT based density increase for the β–γ transition is more reliable than experimentally extrapolated values.

Although calculations of shear moduli and shear velocities are also desirable for completeness, comparisons between computed and observed jumps in the mantle are unlikely to change the present conclusions. Shear moduli and shear velocities should be much more sensitive to temperature, pressure, and probably composition too. The uncertainty in shear velocity will probably be too large to allow one to extract clearer conclusions. Take, for example, the case of the pv–ppv transition (see Wentzcovitch et al., 2006, Fig. 1c). Density and bulk velocity jumps, instead, are much more insensitive, as shown in Fig. 5. Therefore, they are more suitable quantities to investigate if one wants to infer the source of discontinuities. These jumps are some of the most robust results in this paper precisely because they are quite insensitive to pressure and temperature.

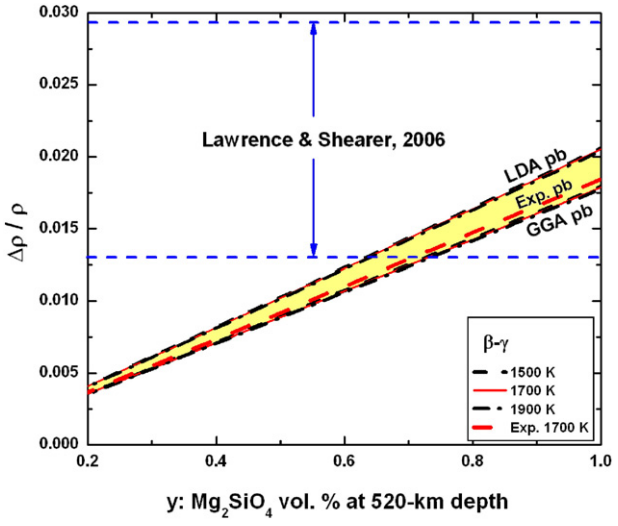

Fig. 7. Density discontinuity produced by the β–γ transition in an aggregate with variable volume fraction of Mg_2SiO_4 in the presence of all other phases (Section 4.2). Results are plotted for three points along the GGA, LDA, and experimental boundary by Katsura and Ito (1989) (Fig. 3(b)) and compared with seismic data by Lawrence and Shearer (2006), wherein the best fit was $\Delta\rho/\rho = 2.1 \pm 0.8\%$.

5. Conclusions and summary

Phase boundaries between α–β–γ Mg_2SiO_4 have been computed from first principles. Uncertainties in the location of these boundaries related to the choice of exchange correlation functional are relatively large. However, the LDA and GGA phase boundaries bracket the experimental ones as found in previous computations of the post-spinel (psp) (Yu et al., 2007) and post-perovskite (ppv) transitions (Tsuchiya et al., 2004). The calculated CSs are in good agreement with experimentally determined values as found earlier for the psp transition and presumably also for the ppv transition. Despite the uncertainty in the phase boundaries, the predicted jumps in ρ, K_S, and V_ϕ have relatively small uncertainties and useful accuracy.

We have estimated the density increases caused by the α–β and β–γ transitions in an aggregate with variable volume fraction of Mg_2SiO_4 assuming that phase transitions in coexisting phases are not sharp and occur over a much wider pressure range. The density jump at 410-km depth marking the upper mantle transition zone boundary can be reproduced by the density discontinuity caused by the α–β transition in an aggregate with pyrolite composition. However, the large uncertainties in the seismic data do not exclude the possibility of accompanying changes in the pyroxene/garnet/Ca-pv system.

The density discontinuity produced by the β–γ transition is relatively small and at least 70 vol.% of Mg_2SiO_4 would be required to reproduce the magnitude of the density discontinuity at 520-km. This strongly suggests that it is necessary to consider contributions from other phase transitions, in addition to the β–γ transition, to understand the nature of the broad (10–50 km width, i.e., 0.4–2 GPa) seismic reflector at 520 km depth (Shearer, 2000). There remain important open questions such as how much other transformations in the pyroxene/garnet/Ca-pv system contribute to the 520-km discontinuity (Weidner and Wang, 2000), and how exactly water partitioning in α–β–γ Mg_2SiO_4 can broaden the 410- and 520-km discontinuities. Further thermodynamic studies of

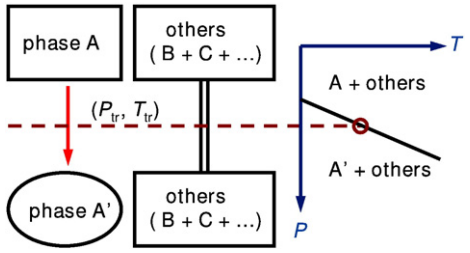

Fig. 8. Model used to compute volume reduction in an aggregate of phases A, B, C, etc., where only phase A undergoes a transition to phase A′.

phase transitions in the pyroxene/garnet/Ca-pv system and their contributions to the 520-km discontinuity are necessary to elucidate these open questions.

Acknowledgments

We thank L. Li for allowing us to compare our forsterite results with hers, C. R. S. da Silva for comments on the manuscript, and S. Zhang for improving the performance of the first principle codes on the blade system at the Minnesota Supercomputing Institute (MSI). We also thank S. V. Sinogeikin and A. Saikia for providing us references which helped the comparison of this study with theirs. This research was supported by NSF/EAR 013533, 0230319, 0635990, and NSF/ITR 0428774 (VLab). Computations were performed at MSI and on the Big Red Cluster at Indiana University.

Appendix A. Density discontinuity due to one phase transformation in an aggregate

Consider an aggregate of phase A, B, C, etc. (Fig. 8). If only phase A undergoes a transition to A′ at (P_{tr}, T_{tr}), then the aggregate density changes by

$$\frac{\Delta\rho}{\rho} \equiv \frac{\rho_{A'+\text{others}} - \rho_{A+\text{others}}}{(\rho_{A'+\text{others}} + \rho_{A+\text{others}})/2}, \tag{A.1}$$

where "others" ≡ B+C+etc. If m is the total mass of the aggregate and V is volume, then

$$\frac{\Delta\rho}{\rho} = \frac{\frac{m}{V_{A'}+V_{\text{others}}} - \frac{m}{V_A+V_{\text{others}}}}{\left(\frac{m}{V_{A'}+V_{\text{others}}} + \frac{m}{V_A+V_{\text{others}}}\right)/2}. \tag{A.2}$$

Let $y = V_A/(V_A+V_{\text{others}})$ and $\theta = V_A/V_{A'}$, then

$$\frac{\Delta\rho}{\rho} = \frac{2y}{\frac{2}{1-\theta} - y}, \tag{A.3}$$

which is Eq. (3) in Section 4.

Appendix B. Thermodynamics of forsterite Mg_2SiO_4

Table B.1
Comparison of forsterite thermodynamic properties in this study (LDA), in Li et al. (2007) (LDA), and in experimental measurements

	V (Å^3)	K_S (GPa)	dK_S/dP	α (10^{-5} K^{-1})	C_P (J/(mol·K))	γ
This work[a]	290.3	127.4	4.3	2.66	119.5	1.25
Li et al. (2007)[a]	289.5	127.6	4.2	2.64	119.3	1.23
This work	285.7[b]	193.9[c]	–	5.10[d]	195.1[d]	–
Exp	285.25(28)[a]	197.54±2.91[b]	–	4.72[c]	199.6[c]	–

a=(300 K, 0 GPa), b=(1371.2 K, 6.6 GPa), c=(300 K, 16.2 GPa), d=(2000 K, 0 GPa).
exp[b]=Meng et al. (1993), exp[c]=Zha et al. (1996), exp[d]=Gillet et al. (1991).

Appendix C. Supplementary data

Supplementary data associated with this article can be found, in the online version, at doi:10.1016/j.epsl.2008.06.023.

References

Agee, C.B., 1998. Phase transformations and seismic structure in the upper mantle and transition zone. In: Hemley, R.J. (Ed.), Ultrahigh-Pressure Mineralogy: Physics and Chemistry of the Earth's Deep Interior. Reviews in Mineralogy, vol. 37, pp. 165–203.
Akaogi, M., Akimoto, S., 1979. High-pressure phase equilibria in a garnet lherzolite, with special reference to Mg^{2+}–Fe^{2+} partitioning among constituent minerals. Phys. Earth Planet. Inter. 19, 31–51.
Akaogi, M., Ito, E., 1993. Refinement of enthalpy measurement of $MgSiO_3$ perovskite and negative pressure–temperature slopes for perovskite-forming reactions. Geophys. Res. Lett. 20, 1839–1842.
Akaogi, M., Ross, N.L., McMillan, P., Navrotsky, A., 1984. The Mg_2SiO_4 polymorphs (olivine, modified spinel and spinel)—thermodynamic properties from oxide melt solution calorimetry, phase relations, and models of lattice vibrations. Am. Mineral. 69, 499–512.
Akaogi, M., Ito, E., Navrotsky, A., 1989. Olivine-modified spinel–spinel transitions in the system Mg_2SiO_4–Fe_2SiO_4: calorimetric measurements, thermochemical calculation, and geophysical application. J. Geophys. Res. 94, 15,671–15,685.
Asada, T., Terakura, K., 1992. Cohesive properties of iron obtained by use of the generalized gradient approximation. Phys. Rev., B 46, 13599–13602 (reference 25).
Baroni, S., de Gironcoli, S., Corso, A.D., Giannozzi, P., 2001. Phonons and related crystal properties from density-functional perturbation theory. Rev. Mod. Phys. 73, 515–562.
Birch, F., 1952. Elasticity and constitution of the Earth's interior. J. Geophys. Res. 57, 227–288.
Brown, J.M., Shankland, T.J., 1981. Thermodynamic parameters in the Earth as determined from seismic profiles. Geophys. J. Int. 66, 579–596.
Canil, D., 1994. Stability of clinopyroxene at pressure–temperature conditions of the transition region. Phys. Earth Planet. Inter. 86 (1–3), 25–34.
Ceperley, D.M., Alder, B.J., 1980. Ground state of the electron gas by a stochastic method. Phys. Rev. Lett. 45, 566–569.
Chopelas, A., 1991. Thermal properties of β-Mg_2SiO_4 at mantle pressures derived from vibrational spectroscopy: implications for the mantle at 400 km depth. J. Geophys. Res. 96, 11817–11829.
Chudinovskikh, L., Boehler, R., 2001. High-pressure polymorphs of olivine and the 660-km seismic discontinuity. Nature 411, 574–577.
Deuss, A., Woodhouse, J., 2001. Seismic observations of splitting of the Mid-Transition Zone discontinuity in Earth's mantle. Science 294, 354–357.
Duffy, T.S., Anderson, D.L., 1989. Seismic velocities in mantle minerals and the mineralogy of the upper mantle. J. Geophys. Res. 94, 1895–1912.
Dziewonski, A.M., Anderson, D.L., 1981. Preliminary reference Earth model. Phys. Earth Planet. Inter. 25, 297–356.
Fei, Y., Van Orman, J., Li, J., van Westrenen, W., Sanloup, C., Minarik, W., Hirose, K., Komabayashi, T., Walter, M., Funakoshi, K., 2004. Experimentally determined postspinel transformation boundary in Mg_2SiO_4 using MgO as an internal pressure standard and its geophysical implications. J. Geophys. Res. (Solid Earth) 109, 2305.
Gaherty, J.B., Wang, Y., Jordan, T.H., Weidner, D.J., 1999. Testing plausible upper mantle compositions using fine-scale models of the 410-km discontinuity. Geophys. Res. Lett. 26, 1641–1644.
Gasparik, T., 1989. Transformation of enstatite–diopside–jadeite pyroxenes to garnet. Contrib. Mineral. Petrol. 102.
Gasparik, T., 1990. Phase relations in the transition zone. J. Geophys. Res. 95, 15751–15769.
Gillet, P., Richet, P., Guyot, F., Fiquet, G., 1991. High-temperature thermodynamic properties of forsterite. J. Geophys. Res. 96, 11805–11816.
Gossler, J., Kind, R., 1996. Seismic evidence for very deep roots of continents. Earth. Planet. Sci. Lett. 138 (1–4), 1–13.
Gu, Y., Dziewonski, A., Agee, C., 1998. Global de-correlation of the topography of transition zone discontinuities. Earth. Planet. Sci. Lett. 157 (1–2), 57–67.
Inoue, T., Irifune, T., Higo, Y., Sanehira, T., Sueda, Y., Yamada, A., Shinmei, T., Yamazaki, D., Ando, J., Funakoshi, K., Utsumi, W., 2006. The phase boundary between wadsleyite and ringwoodite in Mg_2SiO_4 determined by in situ X-ray diffraction. Phys. Chem. Miner. 33, 106–114.
Irifune, T., 1987. An experimental investigation of the pyroxene-garnet transformation in a pyrolite composition and its bearing on the constitution of the mantle. Phys. Earth Planet. Inter. 45, 324–336.
Irifune, T., Susaki, J.-I., Yagi, T., Sawamoto, H., 1989. Phase transformation in diopside $CaMgSi_2O_6$ at pressures up to 25 GPa. Geophys. Res. Lett. 16, 187–190.
Irifune, T., Nishiyama, N., Kuroda, K., Inoue, T., Isshiki, M., Utsumi, W., Funakoshi, K., Urakawa, S., Uchida, T., Katsura, T., Ohtaka, O., 1998. The postspinel phase boundary in Mg_2SiO_4 determined by in situ X-ray diffraction. Science 279, 1698–1700.
Ita, J., Stixrude, L., 1992. Petrology, elasticity, and composition of the mantle transition zone. J. Geophys. Res. 97 (16), 6849–6866.
Ito, E., Takahashi, E., 1989. Postspinel transformations in the system Mg_2SiO_4–Fe_2SiO_4 and some geophysical implications. J. Geophys. Res. 94, 10637–10646.
Jones, L.E., Mori, J., Helmberger, D.V., 1992. Short-period constraints on the proposed transition zone discontinuity. J. Geophys. Res. 97, 8765–8774.
Karki, B.B., Wentzcovitch, R.M., de Gironcoli, S., Baroni, S., 2000a. Ab initio lattice dynamics of $MgSiO_3$ perovskite at high pressure. Phys. Rev., B 62, 14750–14756.
Karki, B.B., Wentzcovitch, R.M., de Gironcoli, S., Baroni, S., 2000b. High-pressure lattice dynamics and thermoelasticity of MgO. Phys. Rev., B 61, 8793–8800.

Katsura, T., Ito, E., 1989. The system Mg_2SiO_4–Fe_2SiO_4 at high pressures and temperatures: precise determination of stabilities of olivine, modified spinel, and spinel. J. Geophys. Res. 94, 15663–15670.

Katsura, T., Yamada, H., Shinmei, T., Kubo, A., Ono, S., Kanzaki, M., Yoneda, A., Walter, M.J., Ito, E., Urakawa, S., Funakoshi, K., Utsumi, W., 2003. Post-spinel transition in Mg_2SiO_4 determined by high P–T in situ X-ray diffractometry. Phys. Earth Planet. Inter. 136, 11–24.

Katsura, T., Yamada, H., Nishikawa, O., Song, M., Kubo, A., Shinmei, T., Yokoshi, S., Aizawa, Y., Yoshino, T., Walter, M.J., Ito, E., Funakoshi, K.-i., 2004. Olivine-wadsleyite transition in the system $(Mg,Fe)_2SiO_4$. J. Geophys. Res. 109, 2209.

Kiefer, B., Wentzcovitch, R.M., Stixrude, L., 1999. Normal and inverse ringwoodite at high pressures. Am. Mineral. 84, 288–293.

Kohn, W., Sham, L.J., 1965. Self-consistent equations including exchange and correlation effects. Phys. Rev. 140, 1133–1138.

Koito, S., Akaogi, M., Kubota, O., Suzuki, T., 2000. Calorimetric measurements of perovskites in the system $CaTiO_3$–$CaSiO_3$ and experimental and calculated phase equilibria for high-pressure dissociation of diopside. Phys. Earth Planet. Inter. 120, 1–2.

Lawrence, J.F., Shearer, P.M., 2006. Constraining seismic velocity and density for the mantle transition zone with reflected and transmitted waveforms. Geochem. Geophys. Geosyst. 7, Q10012.

Li, B., Liebermann, R.C., 2007. Indoor seismology by probing the Earth's interior by using sound velocity measurements at high pressures and temperatures. Proc. Natl. Acad. Sci. U. S. A. 9145–9150.

Li, L., Wentzcovitch, R.M., Weidner, D.J., Da Silva, C.R.S., 2007. Vibrational and thermodynamic properties of forsterite at mantle conditions. J. Geophys. Res. 112, B05206.

Litasov, K., Ohtani, E., Sano, A., Suzuki, A., Funakoshi, K., 2005. In situ X-ray diffraction study of post-spinel transformation in a peridotite mantle: implication for the 660-km discontinuity [rapid communication]. Earth. Planet. Sci. Lett. 238, 311–328.

Matsuzaka, K., Akaogi, M., Suzuki, T., Suda, T., 2000. Mg–Fe partitioning between silicate spinel and magnesiowüstite at high pressure: experimental determination and calculation of phase relations in the system Mg_2SiO_4–Fe_2SiO_4. Phys. Chem. Miner. 27, 310–319.

Meng, Y., Weidner, D.J., Gwanmesia, G.D., Lieberman, R.C., Vaughan, M.T., Wang, Y., Leinenweber, K., Pacalo, R.E., Yeganeh-Haeri, A., Zhao, Y., 1993. In situ high P–T X ray diffraction studies on three polymorphs (α, β, γ) of Mg_2SiO_4. J. Geophys. Res. 98, 22199–22207.

Monkhorst, H.J., Pack, J.D., 1976. Special points for Brillouin-zone integrations. Phys. Rev., B 13, 5188–5192.

Morishima, H., Kato, T., Suto, M., Ohtani, E., Urakawa, S., Utsumi, W., Shimomura, O., Kikegawa, T., 1994. The phase boundary between α- and β-Mg_2SiO_4 determined by in situ X-ray observation. Science 265, 1202–1203.

Navrotsky, A., 1980. Lower mantle phase transitions may generally have negative pressure–temperature slopes. Geophys. Res. Lett. 7, 709–712.

O'Neill, H.S.C., Navrotsky, A., 1983. Simple spinels; crystallographic parameters, cation radii, lattice energies, and cation distribution. Am. Mineral. 89, 181–194.

Ohtani, E., Litasov, K.D., 2006. The effect of water on mantle phase transitions. Reviews in Mineralogy and Geochemistry, vol. 62, pp. 397–420.

Perdew, J.P., Burke, K., Ernzerhof, M., 1996. Generalized gradient approximation made simple. Phys. Rev. Lett. 77, 3865–3868.

Price, G.D., Parker, S.C., Leslie, M., 1987. The lattice dynamics and thermodynamics of the Mg_2SiO_4 polymorphs. Phys. Chem. Miner. 15 (2), 181–190.

Revenaugh, J., Jordan, T.H., 1991. Mantle layering from ScS reverberations. 2. The transition zone. J. Geophys. Res. 96 (B12), 19763–19780.

Rigden, S.M., Fitz Gerald, J.D., Jackson, I., Gwanmesia, G.D., Liebermann, R.C., 1991. Spinel elasticity and seismic structure of the transition zone of the mantle. Nature 354, 143–145.

Ringwood, A.E., 1975. Composition and Petrology of the Earth's Mantle. McGraw-Hill, New York. Ch. 14-3.

Ringwood, A.E., Major, A., 1970. The system Mg_2SiO_4–Fe_2SiO_4 at high pressures and temperatures. Phys. Earth Planet. Inter. 3, 89–108.

Ryberg, T., Wenzel, F., Egorkin, A.V., Solodilov, L., 1997. Short-period observation of the 520 km discontinuity in northern Eurasia. J. Geophys. Res. 102, 5413–5422.

Saikia, A., Frost, D.J., Rubie, D.C., 2008. Splitting of the 520-kilometer seismic discontinuity and chemical heterogeneity in the mantle. Science 319 (5869), 1515–1518.

Shearer, P.M., 1990. Seismic imaging of upper-mantle structure with new evidence for a 520-km discontinuity. Nature 344 (6262), 121–126.

Shearer, P.M., 2000. Upper mantle seismic discontinuities. Earth's Deep Interior: Mineral Physics and Tomography from the Atomic to the Global Scale. Geophysical Monograph, vol. 117, pp. 115–131.

Shearer, P.M., Flanagan, M.P., 1999. Seismic velocity and density jumps across the 410- and 660-kilometer discontinuities. Science 285 (5433), 1545–1548.

Shim, S.N., Duffy, T.S., Shen, G., 2001. The post-spinel transformation in Mg_2SiO_4 and its relation to the 660-km seismic discontinuity. Nature 411, 571–574.

Sinogeikin, S.V., Bass, J.D., Katsura, T., 2003. Single-crystal elasticity of ringwoodite to high pressures and high temperatures: implications for 520 km seismic discontinuity. Phys. Earth Planet. Inter. 136, 41–66.

Stixrude, L., 1997. Structure and sharpness of phase transitions and mantle discontinuities. J. Geophys. Res. 102, 14835–14852.

Stixrude, L., Bukowinski, M.S.T., 1993. Thermodynamic analysis of the system MgO–FeO–SiO_2 at high pressure and the structure of the lowermost mantle. Evolution of the Earth and Planets, pp. 131–141.

Stixrude, L., Lithgow-Bertelloni, C., 2005a. Mineralogy and elasticity of the oceanic upper mantle: origin of the low-velocity zone. J. Geophys. Res. 110, B3204.

Stixrude, L., Lithgow-Bertelloni, C., 2005b. Thermodynamics of mantle minerals—I. Physical properties. Geophys. J. Int. 162, 610–632.

Suito, K., 1977. Phase relations of pure Mg_2SiO_4 up to 200 kilobars. In: Manghnani, M.H., Akimoto, S. (Eds.), High Pressure Research—Applications to Geophysics. Academic Press, New York, pp. 255–266.

Suzuki, A., Ohtani, E., Morishima, H., Kubo, T., Kanbe, Y., Kondo, T., Okada, T., Terasaki, H., Kato, T., Kikegawa, T., 2000. In situ determination of the phase boundary between wadsleyite and ringwoodite in Mg_2SiO_4. Geophys. Res. Lett. 27, 803–806.

Tsuchiya, T., Tsuchiya, J., Umemoto, K., Wentzcovitch, R.M., 2004. Phase transition in $MgSiO_3$ perovskite in the earth's lower mantle. Earth. Planet. Sci. Lett. 224, 241–248.

Weidner, D.J., Wang, Y., 2000. Phase transformations: implications for mantle structure. Earth's Deep Interior: Mineral Physics and Tomography from the Atomic to the Global Scale. Geophysical Monograph, vol. 117, pp. 215–235.

Wentzcovitch, R.M., 1991. Invariant molecular-dynamics approach to structural phase transitions. Phys. Rev., B 44, 2358–2361.

Wentzcovitch, R.M., Karki, B.B., Cococcioni, M., de Gironcoli, S., 2004. Thermoelastic properties of $MgSiO_3$-perovskite: insights on the nature of the Earth's lower mantle. Phys. Rev. Lett. 92 (1), 018501.

Wentzcovitch, R.M., Tsuchiya, T., Tsuchiya, J., 2006. $MgSiO_3$ postperovskite at D″ conditions. Proc. Natl. Acad. Sci. U. S. A. 103 (3), 543–546.

Wiggins, R.A., Helmberger, D.V., 1973. Upper mantle structure of the western United States. J. Geophys. Res. 78, 1870–1880.

Wu, Z., Wentzcovitch, R.M., 2007. Vibrational and thermodynamic properties of wadsleyite: a density functional study. J. Geophys. Res. 112, B12202.

Yagi, T., Bell, P.M., Mao, H.K., 1979. Phase relations in the system MgO–FeO–SiO_2 between 150–170 kbar at 1000 °C. Year Book Carnegie Inst., vol. 78, pp. 614–618. Washington.

Yu, Y.G., Wentzcovitch, R.M., 2006. Density functional study of vibrational and thermodynamic properties of ringwoodite. J. Geophys. Res. 111, B12202.

Yu, Y.G., Wentzcovitch, R.M., Tsuchiya, T., Umemoto, K., Weidner, D.J., 2007. First principles investigation of the postspinel transition in Mg_2SiO_4. Geophys. Res. Lett. 34, 10306.

Zha, C.-S., Duffy, T.S., Downs, R.T., Mao, H.-K., Hemley, R.J., 1996. Sound velocity and elasticity of single-crystal forsterite to 16 GPa. J. Geophys. Res. 101, 17535–17546.